applied sciences

MDPI

Article

A Numerical Aerodynamic Analysis on the Effect of Rear Underbody Diffusers on Road Cars

Alex Guerrero *,†, Robert Castilla and Giorgio Eid †

CATMech—Centre for Advanced Technologies in Mechanics, Universitat Politecnica de Catalunya, Catalunya, 08222 Terrassa, Spain; robert.castilla@upc.edu (R.C.); giorgio.eid@mail.polimi.it (G.E.)

* Correspondence: alex.guerrero@mail.polimi.it

† Current address: Politecnico di Milano, Scuola di Ingegneria Industriale e dell'Informazione, 20133 Milan, Italy.

Abstract: The aerodynamic complexity of the underbody surfaces of conventional road vehicles is a matter of fact. Currently available literature is focused mainly on very simple Ahmed-body geometries as opposed to realistic car shapes, due to their complexity and computational cost. We attempted to understand the flow behaviour around different realistic conventional road car geometries, and we provide an extensive evaluation of the aerodynamic loads generated. The key findings of this article could potentially set a precedent and be useful within the automotive industry's investigations on drag-reduction mechanisms or sources of downforce generation. The novelty of the work resides in the realistic approach employed for the geometries and in the investigation of barely researched aerodynamic elements, such as front diffusers, which might pave the way for further research studies. A baseline flat-underfloor design, a 7° venturi diffuser-equipped setup, a venturi diffuser with diagonal skirts, and the same venturi diffuser with frontal slot-diffusers are the main configurations we studied. The numerical predictions evaluated using RANS computational fluid dynamics (CFD) simulations deal with the aerodynamic coefficients. The configuration that produced the highest downforce coefficient was the one composed of the 7° venturi diffuser equipped with diagonal sealing skirts, achieving a C_L value of −0.887, which represents an increase of around 1780% with regard to the baseline model. That achievement and the gains in higher vertical loads also entail a compromise with an increase in the overall air resistance. The performance achieved with diffusers in the generation of downforce is, as opposed to the one obtained with conventional wings, a cleaner alternative, by avoiding wake disturbances and downwash phenomena.

Keywords: computational fluid dynamics; CFD; diffusers; downforce; drag; external aerodynamics; incompressible flow; openfoam; simplefoam; underbody; vortex; wake

Citation: Guerrero, A.; Castilla, R.; Eid, G. A Numerical Aerodynamic Analysis on the Effect of Rear Underbody Diffusers on Road Cars. *Appl. Sci.* **2022**, *12*, 3763. https://doi.org/10.3390/app12083763

Academic Editor: Artur Tyliszczak

Received: 9 March 2022
Accepted: 30 March 2022
Published: 8 April 2022

1. Introduction

A proper and adequate design of the underbody of a road car is by no means an easy task, and usually represents a resource-demanding duty for aerodynamicists and car manufacturers. The high complexity of incompressible but turbulent flows observed around a sophisticated and detailed underbody of a road vehicle may generate notorious and undesired air resistance that in turn will cause a non-subtle increase in the fuel consumption [1]. In fact, aerodynamic drag is responsible for more than 50% of the propulsive fuel consumption of a typical car running on a highway [2]. Moreover, it has been shown that a reduction in aerodynamic drag specifically is achievable at a relatively low cost compared to improving other car mechanisms, such as the development of a more efficient power train system; therefore, it is an economical target [3].

Some publications, such as the works of Alkan [4] and Copper et al. [5], suggest that some acoustic phenomena may also be originated as a result of a poor underbody treatment when conceiving of the designs of road cars. Again, the complex wake and strong vorticity that are generated due to the underfloor being in the vicinity of problematic rotating elements, such as wheels, deserve special attention and study.

The evolution of underbodies and diffusers in the automotive sector cannot be explained without the contributions of several motorsport categories, such as Can-Am and Formula One, where the works of Jim Hall and Colin Chapman (among others) traced the paths for future aerodynamic development.

Over the years, multiple body shapes for race cars have been conceptualised to create downforce with minimal drag-induced penalties. For an example, see the basic catamaran shape illustrated in Figure 1.

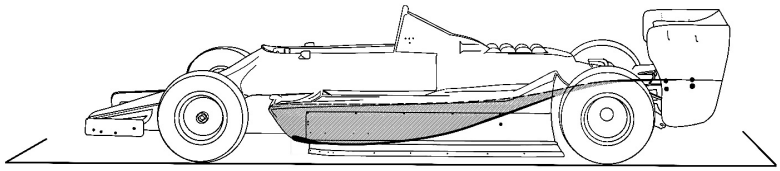

Figure 1. Basic catamaran body shape.

The core shape covers the wheels. There is a central channel with an offset from the ground that ends in a venturi qualified by an upward rear slope. The goal is to maintain an undisturbed free stream under the car and prevent flow separation at the rear end [6].

Furthermore, some studies of ground effect diffusers have been performed to improve performance due to the major aerodynamic contribution of the diffusers to downforce generation (up to 50%) [7]. This effect is due to the longitudinal counter-rotating vortices generated that roll up along the diffuser's endplates within the diffuser's flow channel, which enhances suction by accelerating the streamwise diffuser flow.

In recent years, the easy access to CFD solvers [8] and the generalisation of wind tunnel testing [9] has allowed interesting research and publications. Generalised geometries such as the *Ahmed Body* have been extensively evaluated. A pertinent example is the study of the coherent flow structures generated in the wake of the Ahmed body. Effectively, a recirculating bubble over the slanted surface can be distinguished, along with longitudinal C-Pillar vortices originating from the side edges of the rear window and a recirculation torus behind the vertical base [10].

Another remarkable study was presented by Hucho [11], where rear flow separation was evaluated as a function of slant angle. The analysis of the flow depicts two primary types of vortices in the wake: a ring vortex, running perpendicularly to the flow direction, and a longitudinal horseshoe-shaped vortex, which is associated with a large increase in drag. The relevant idea was to use the car's geometry to counteract these vortices by modifying the slant angle.

Some studies have also been conducted on diverse aerodynamic passive control devices, for instance, splitter plates [12] and flaps [13,14]. However, sometimes disagreements have been encountered regarding the aesthetics and the performances of the cars, and these concepts were not applied.

Other experimental approaches, such as the one led by Zhang et al. [15], have evaluated the usage of sealing skirts on the underbody to channelise and direct the flow towards the exit diffuser section. The latter, along with a proper diffuser angle, can provide a significant 32.5% increase in the downforce coefficient when compared to a baseline model. Another investigation on an Ahmed bluff body at a 0° upper slant angle that had a diffuser with side plates was performed to elaborate the different types of flow regions for the configuration [16].

More advanced methods were used in some studies to improve diffuser performance. For instance, an artificial neural network was used for the aerodynamic optimisation of a sedan. Using this technique, the drag coefficient was improved by 5.64% with respect to the baseline model, demonstrating the importance of the rear-end aerodynamics for a standard sedan-like vehicle [17].

The following subsection is aimed at reviewing the fundamental theory and literature available about the addition of diffusers to the underbodies of automotive vehicles.

1.1. Literature Review and Diffusers' Fundamental Theory

As explicitly stated by Filipe et al. [18], diffusers may easily be understood as aerodynamic elements, usually mounted on the rear area of the underbody of a ground transport vehicle, whose main function is to increase the downforce and facilitate a smooth transition from the underbody flow back to free stream conditions.

The downforce on the underbody area is created mainly due to the presence of a suction area originated by a Venturi's effect, which in turn is greatly intensified with the presence of a diffuser. This process mimics the flow over a constricted tube as shown in Figure 2, interpreted from [1]. The role of the diffuser is to raise the low pressure of the air underneath the car back to atmospheric pressure.

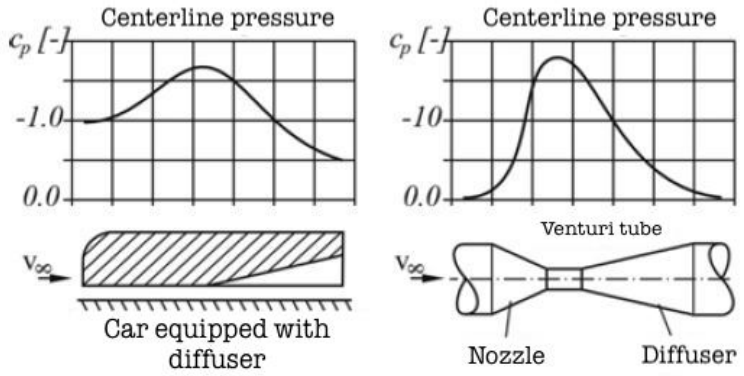

Figure 2. Pressure distribution along the centreline of a generic body of car with an underbody diffuser and a Venturi tube.

The slope of the diffuser is critical to increasing the flow speed and reducing the pressure locally [19], and that is why the diffuser also acts as an expansion chamber to smoothly recover the free stream conditions from the vehicle's influence. By smoothing this transition, turbulence and drag in the vehicle's wake are improved. Figure 3 shows the adoption of a typical diffuser automotive's configuration.

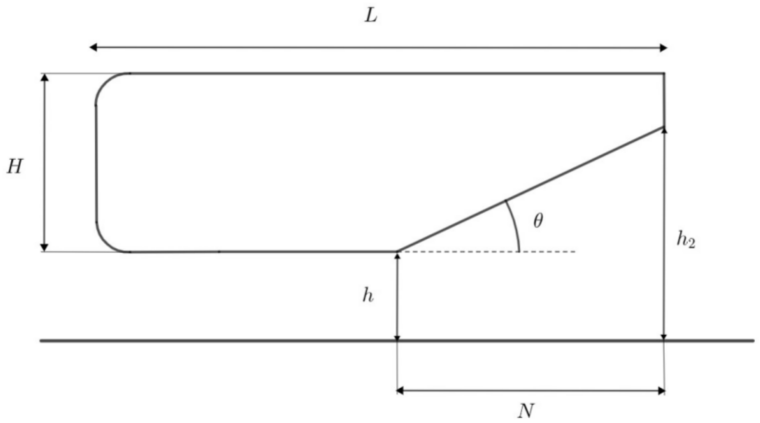

Figure 3. Schematic representation of a bluff body with an added diffuser [8].

Again, the works of Copper et al. [20] reflect some fundamental fluid-mechanical sources of downforce found when evaluating closely the flow behaviour of diffusers.

If a perfectly symmetric bluff body at the zero-angle of attack, such as the *Ahmed body*, is considered for evaluation, it will be clearly visible that no downforce is generated due to it not generating any pressure differential between the upper and lower surfaces, just as in a symmetric airfoil.

However, when testing the body close to the ground, the airflow under the body experiences an increase in its velocity caused by the ground constraint, a phenomena called

ground interaction. This phenomenon has been studied rigorously in vehicle aerodynamics [16]. Descriptions of the major flow structures for different ride heights have been obtained, along with insights on the flow's physics. The acceleration of the flow because of the ground effect causes, in turn, a pressure gradient between the upper and lower surface, and originates a resulting aerodynamic lifting force, as seen in [21]. Figure 4 shows the variation in the loads generated at different ride heights. It is important to note that such an increase in downforce when decreasing the ride height is limited due to fluid viscosity. These viscous effects are not dominant at large ride heights; therefore, downforce reaches its maximum at a certain low ride height, as stated by Unni [22].

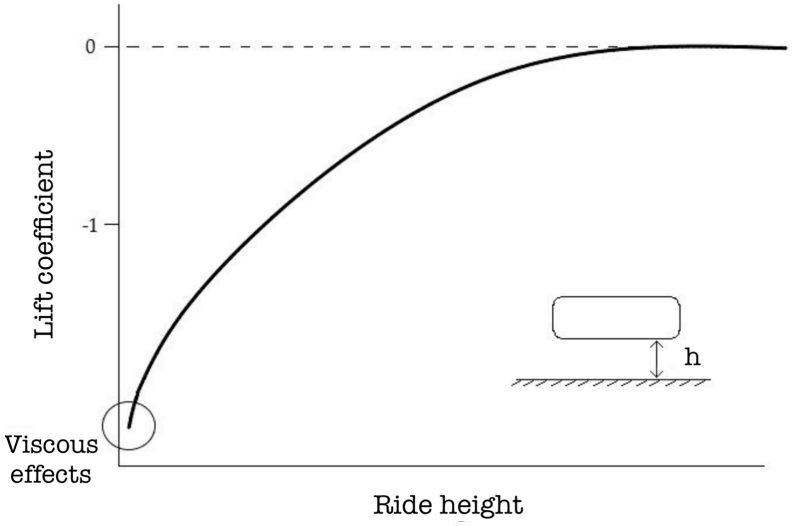

Figure 4. Downforce generation at different ride heights [8].

The second mechanism for the generation of downforce on the underbody is the curved non-symmetrical zones at the rear of the body. That cambered shape creates a flow asymmetry that gives rise to the apparition of a suction peak at the inlet of the diffuser. Nonetheless, it is extremely important to model and design the diffuser angle θ to avoid flow separation, which is mathematically expressed by an adverse pressure gradient in the axial flow direction.

To prevent flow separation in an expanding rectangular duct, an equivalent conical section is calculated, based on relevant length, inlet, and outlet areas [23]. This angle must normally not exceed 7°, to avoid flow separation [24]. Nevertheless, racing diffusers can achieve attached flow with angles superior to 20° [25], but it is typically accepted that the optimum value is often found around 7° [26]. The cambered geometry of the diffuser counters the non-clockwise, rotating, streamwise vortical structure pair upward, created by the pressure gradient between the diffuser and the outer region [7].

It is interesting to note that the contribution of Tian [27] describes perfectly the flow behaviour under the surface of a diffuser-equipped geometry in terms of pressure coefficient (see Equation (1)).

$$C_p = 1 - \frac{U}{U_\infty} \tag{1}$$

As can be observed in Figure 5, interpreted from [28], that the flow experiences an acceleration after the inlet of the underbody (low-pressure zone) for both cases, the baseline and the diffuser setting. That zone is followed by a pressure recovery phenomenon [18] that finally adopts the free stream pressure value. The main difference is that for the flat underbody, that process is undertaken continuously, whereas for the diffuser configuration it is done in two stages, where a pressure peak is found. Through the diffuser, a portion of the kinetic energy of the fluid is turned into potential pressure energy, also called pumping effect, as described in [29]. The pressure drop at the exit is almost identical for both cases, but the lower it is, the less drag it would cause, since vorticity would be smaller. Hence,

diffusers may also be employed adequately with the idea of controlling the boundary layer separation of the flow on the undertray. This can, if done properly, avoid the large turbulence phenomenon of the wake.

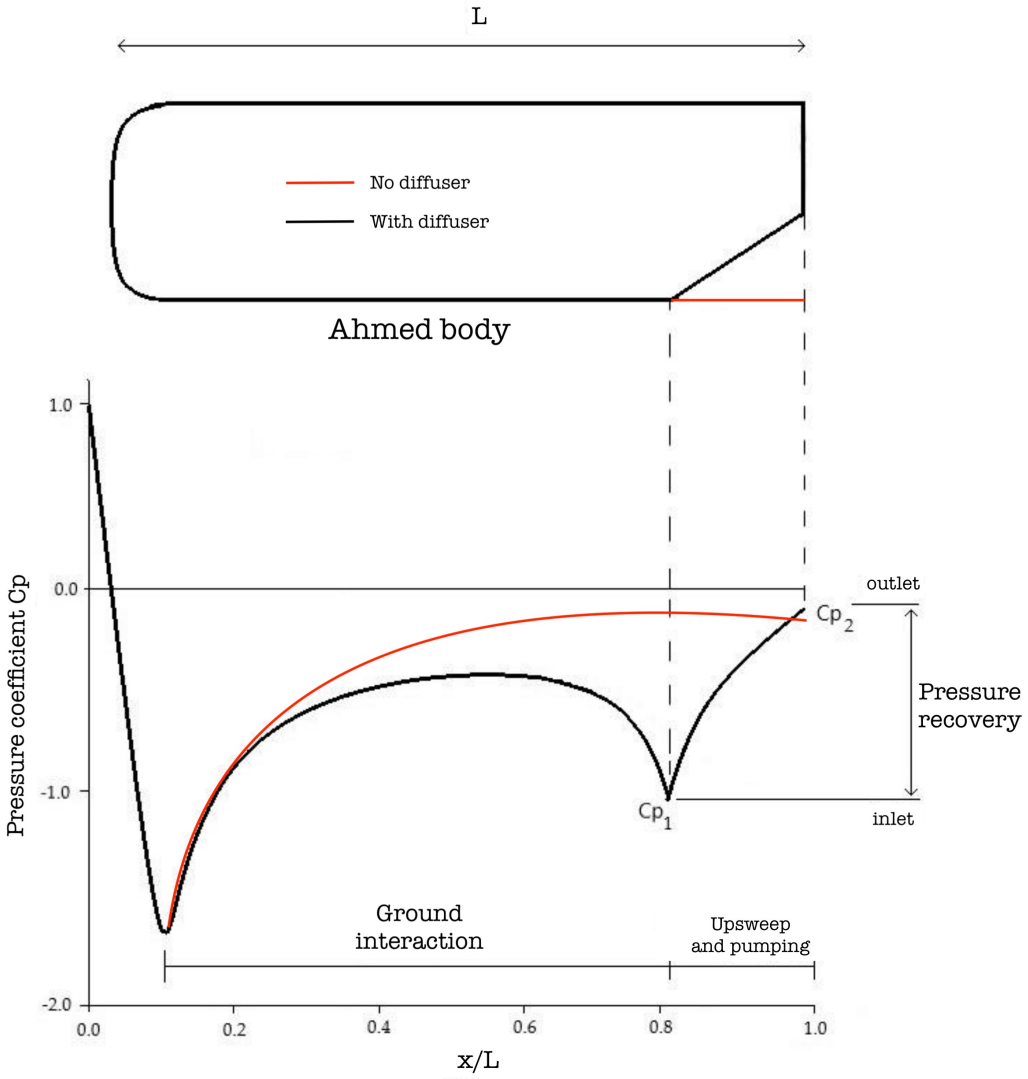

Figure 5. Pressure coefficient curve around a bluff body.

Various additional elements have been studied to improve the aerodynamic performances of vehicles. Examples of such research are presented in [30]: the analysis of a bluff body shaped underbody diffuser with side plates and moving ground. The conclusion drawn was that the diffuser can benefit the drag reduction of the body and the correct upper slant angle can enhance the improvement. More ambitious projects were also done with active flow control devices such as pulsed jets activation and decreased the drag by about 6–8% [31]. In the work of Kang et al. [32] the concept of actively translating diffusers was introduced, as can be seen in Figure 6. When active, within the range of 70–160 km/h, drag was reduced by about 4%, as the diffuser blocked the low-pressure air from the underbody, which filled the rear end with high pressure from the sides, consequently raising the base pressure of the car and creating a smoother recovery.

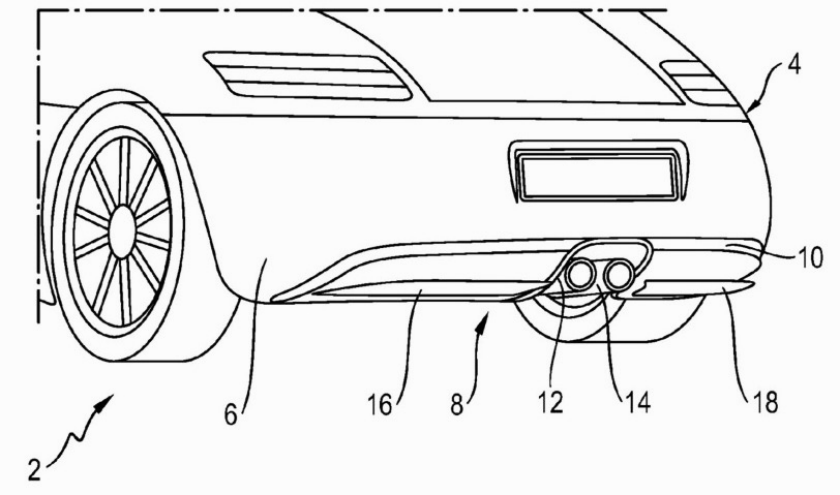

Figure 6. Active diffuser scheme of a Porsche car [33].

Before proceeding to the analysis of the diffuser of this paperwork, it is relevant to contemplate the physics of the flow involved in the relevant flow. Therefore, an adequate reference is an investigation of the aerodynamic behaviour of an underbody diffuser fitted to a wind tunnel model of a wheel-less, simple body of passenger car proportions [5]. The three major aerodynamic phenomenona are hence identified and explained: first, the ground effect previously mentioned as a consequence of the asymmetry of the flow; then, the upsweep of the rear underbody produces the effect of a camber, resulting in significant downforce; finally, the pumping effect of the diffuser, which naturally accelerates the flow because of its geometry. Moreover, in a subsequent study [20], an analytical model based on a simple diffuser/body combination was developed to generalise the experiment. It was demonstrated that an effective underbody can include a relatively short diffuser (half of the length of the underbody), that the optimum diffuser length decreases as the area ratio of the diffuser decreases, and that the optimum area increases as the ride height increases.

An interesting example from race car optimisation via the adjoint method has been reported in [34]. The results can be seen in Figure 7. In fact, after adding the diffuser, the larger longitudinal vortices of the wake were reduced and dissipated earlier because of the underbody-induced counter-rotating vortices, which led to a significant drag reduction.

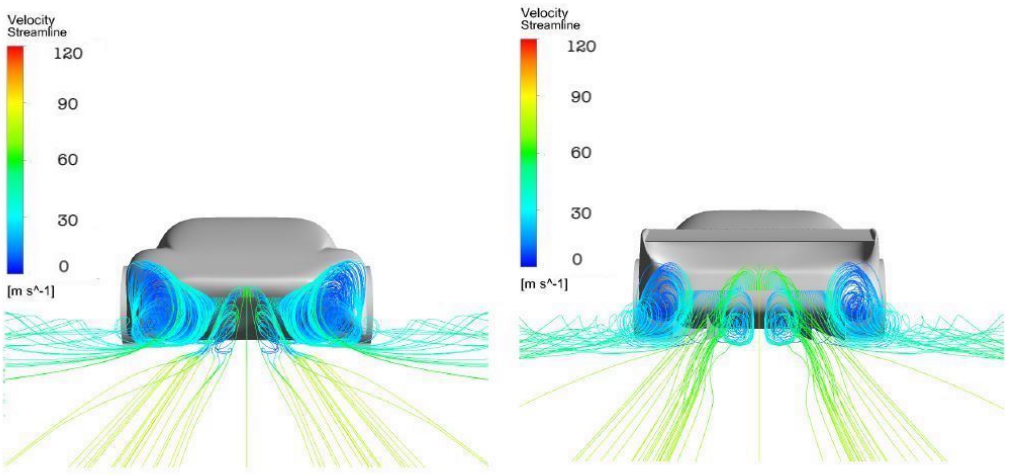

(a) Iteration 0. (b) Iteration 2.

Figure 7. Wake vorticity comparison after using the adjoint solver [34].

In addition, some studies on the relationship between the reversal zone behind the body and the diffuser upsweeping angle at a fixed slant angle yielded relevant results on

the flow. In fact, in [17] it is shown that the reversal zone moves upward with the increase in upsweeping angle and that the turbulent kinetic energy density follows the same trend. In conjunction with the effect of the counter-rotating vortices generated by the diffuser, a reduction in turbulence behind the car can be achieved which grants a reduction in vortex intensity, better pressure recovery, and thus less drag.

The last important consideration is the effect of the presence of the wheels in proximity of the diffuser. Since they are rotating elements, which greatly interfere with the flow, their effect is considerable. Indeed, for a body without wheels, this study reveals that there would be continuous and predictable variations in lift and drag for an angle of the diffuser of $\alpha \leq 7°$. Above this value, separation of the airstream might occur because of the growth of vortex structure generated by lateral inflows on the sides of the diffuser surface into the underbody region, which can significantly alter the flow behind the body [35]. A subsequent study on a hatchback car with wheels at varying diffuser lengths and angles was done afterwards [36]. It was concluded that the vortices originating from the wheelhouse have a significant effect on the aerodynamic loads of the car, and that there is a possibility of reaching a minimal drag by choosing the right diffuser combination.

The key factor to choose is the diffuser angle, which focuses on the diffuser itself and additional underbody elements. To achieve this purpose, some studies on the diffuser angle's effect on the flow are considered.

A particularly pertinent work is presented in [37]. The authors studied the flow over a diffuser at angles of 5, 10, 15, 17, and 20°. The results for the 5, 10, and 15° cases are shown in Figure 8. It was observed that for the 5° case, there was no separation bubble and the flow was slow and unsteady at the exit. For the 10° case, the separation bubble formed at the inlet and closed just ahead of the outlet with something similar to the onset of a longitudinal vortex breakdown. For the three remaining cases, the separation bubble was closer to the inlet, and since it was open, the vortex breakdown happened earlier. Therefore, since the first case was not prone to separation and the second case was deemed transitional, for this study the diffuser angle was chosen to be inferior to 10°.

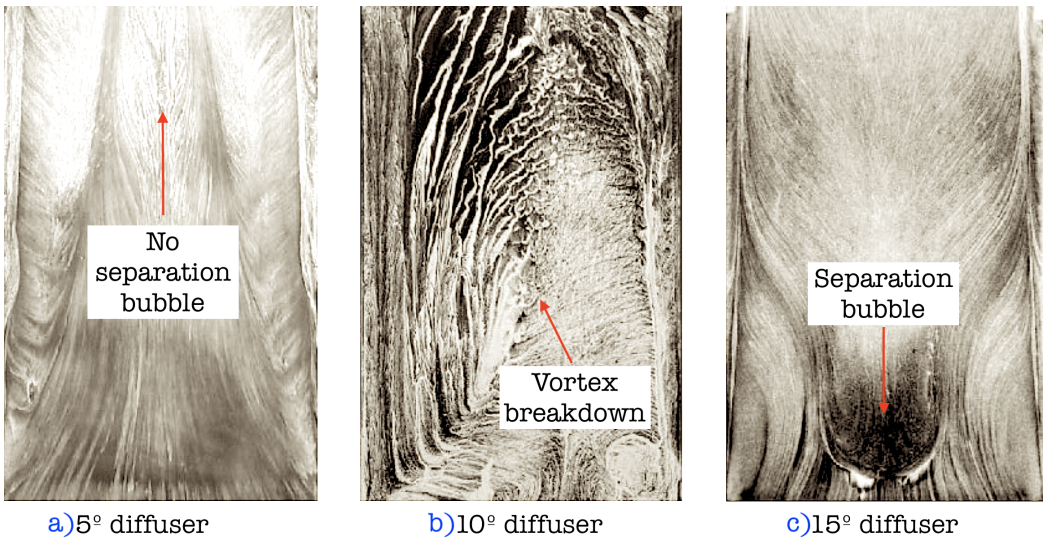

Figure 8. Surface flow visualisation at diffuser angles of (**a**) 5°, (**b**) 10° and (**c**) 15° (Reprinted with permission from the University of Southampton [15]).

Furthermore, in the works of Alkan [4], study to reduce the drag of a sedan car was performed by CFD for various diffuser angles, and it was demonstrated that the drag coefficient decreased as the diffuser angle increased, until a limit of approximately 7°. This is the consequence of an increased underbody mass flow, which leads to better velocity recovery, and this effect is eliminated at larger diffuser angles because of separated flow. In addition, in an investigation on using diffusers for maximal downforce to reduce incidents on highways [38], it was shown that for a 7° angle there is an improvement in drag

coefficient with respect to the other choices of at least 1.3–1.4% and that for angles superior to 10°, flow might separate, since the separation bubble is near opening at such angle. Lastly, through research done on a modified diffuser geometry with a varying angle for the diffuser plates [39], it has been shown that for angles lower than 8° the improvements in aerodynamic coefficients can reach up to 8% for lift and 2.5% for drag. This motivated the use of diagonal skirts within this study to improve aerodynamic performance.

1.2. Aim of the Work and Justification

After a deep review of the existent and current literature, we found it appropriate to perform a numerical aerodynamic study to evaluate the flow behaviour around a conventional road car and to quantify and evaluate the aerodynamic forces that are generated. Different aerodynamic configurations regarding the addition of diffuser-like elements were tested and compared to a baseline unaltered configuration. The purpose was to offer a broad overview of the underbody aerodynamic phenomena that are present in conventional road cars and understand the basic drag-reduction mechanisms and downforce-generation sources.

The flow behaviour and similarities with the Ahmed body are key factors to bear in mind in order to understand and properly describe the solution to the problem.

However, the novelty and originality of the present work reside in the fact that it is based on a more realistic approach of a road car than a simple Ahmed body. The realistic windshield curvature, a semi-flat underbody, and the addition of rotating wheels offer a notable step forward in the quality, usefulness, and realism of the results. In addition, the diffusers contain flow vanes and vertical fences, which again offers a more realistic treatment of the different flow natures developed on the underbody of a car.

On the other hand, front diffuser-like elements are extremely rarely described in the available literature. The front diffuser design and sealing skirts adaptation are original, meet the criteria, and show our expertise in the field.

Therefore, the contributions of this paper could potentially set a precedent for further studies on this matter and provide insights into the potential of these aerodynamic elements on road cars.

2. Materials and Methods

2.1. Geometry

Several three-dimensional CFD simulations were performed on a self-designed road car geometry. The configurations designed comprise the baseline model (with a flat underfloor) and three configurations with additions:

- Venturi diffuser: uses a 7° angle diffuser on the rear of the baseline model.
- Venturi skirts: uses the Venturi diffuser configuration with the addition of diagonal sealing skirts on the underbody to channelise and guide the flow towards the diffuser area.
- Venturi frontal diffuser: again, uses the Venturi diffuser configuration, along with two small frontal diffuser sections in front of the region of the tires.

Figure 9 shows the baseline CAD model utilised for the main configuration. The wheelbase of the model is around 2.45 m; the total length of the car is 4 m. Figure 10 shows the diffuser. Figure 11 displays the front diffusers and diagonal skirts employed on the other configurations.

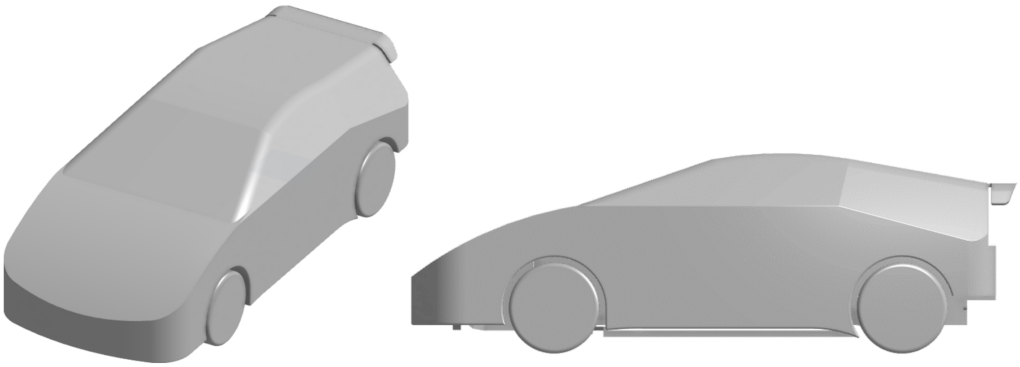

Figure 9. Trimetric and side view of the baseline model (flat underbody).

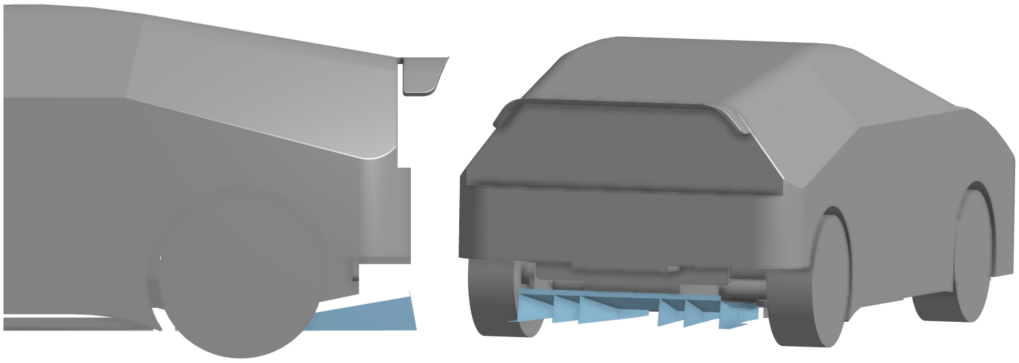

Figure 10. Side and rear view of the diffuser mounted on any of the configurations with additions.

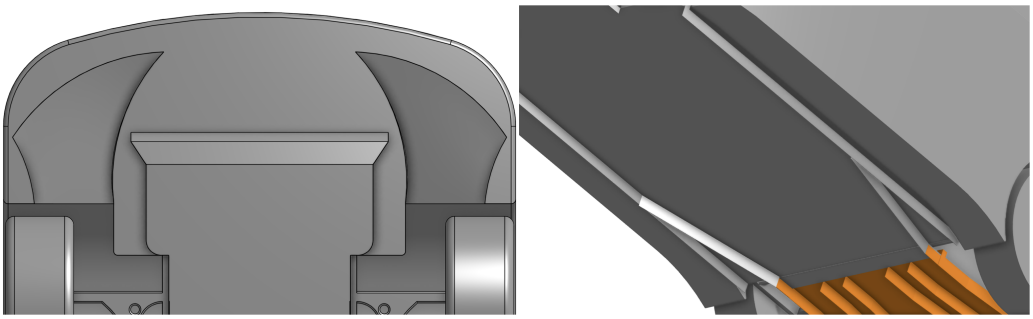

Figure 11. Bottom and inclined view of the front diffusers and diagonal sealing skirts, respectively.

2.2. Solver

The RANS simulations were carried out using the OpenFoam toolbox, which solves the equations for steady-state incompressible flow of mass and momentum (see Equation (2)), referred to as Navier–Stokes equations [40]; and the continuity equation shown in Equations (2) and (3). This mathematical RANS formulation employed as the goal not studying transient phenomena [41] (which could be the subject of future work), but the averages to evaluate the effect on the average performance of the car, as stated in [21].

$$\rho \frac{\partial \mathrm{u}}{\partial t} + \rho(\mathrm{u} \cdot \nabla)\mathrm{u} = -\nabla p + \mu \Delta \mathrm{u} \tag{2}$$

where:

$$\triangle \equiv \nabla^2 = \frac{\partial^2}{\partial x^2} + \frac{\partial^2}{\partial y^2} + \frac{\partial^2}{\partial z^2}$$

$$\nabla \mathrm{u} = 0 \tag{3}$$

The whole domain's discretisation was performed using the FVM (Finite Volume Method), a locally conservative approach due to being based on a balanced method [42]. For the gradients, divergence, and laplacian terms, the Gaussian schemes were used; resulting in linear upwind second-order interpolation schemes at cell interfaces.

The solver chosen was the simpleFoam algorithm (semi-implicit method for pressure-linked equations), a reasonable approach to an incompressible, steady-state turbulent flow. Considering that the study aimed to evaluate the mean flow parameters rather than to study the evolution of the temporal formation of transient eddies, this is considered the most adequate approach. The GAMG (geometric algebraic multigrid) was selected for the pressure equation, and smoothSolver was selected for velocity and turbulent physical parameters [41].

Finally, the turbulence model chosen was k-ω SST (k-ϵ was employed in the outer region of and outside of the boundary layer and k-ω was employed in the inner boundary layer), as it benefits from a two-equation model offering more accurate results when compared to other models, i.e., Spalart Allmaras [43].

2.3. Domain and Mesh

The overall dimensions of the problem's domain were inspired by the works of Broniszewski et al. [41,44], who placed a special emphasis on the outer rear region of the car to capture the wake's generation adequately. Figure 12 reflects the boundaries of the domain.

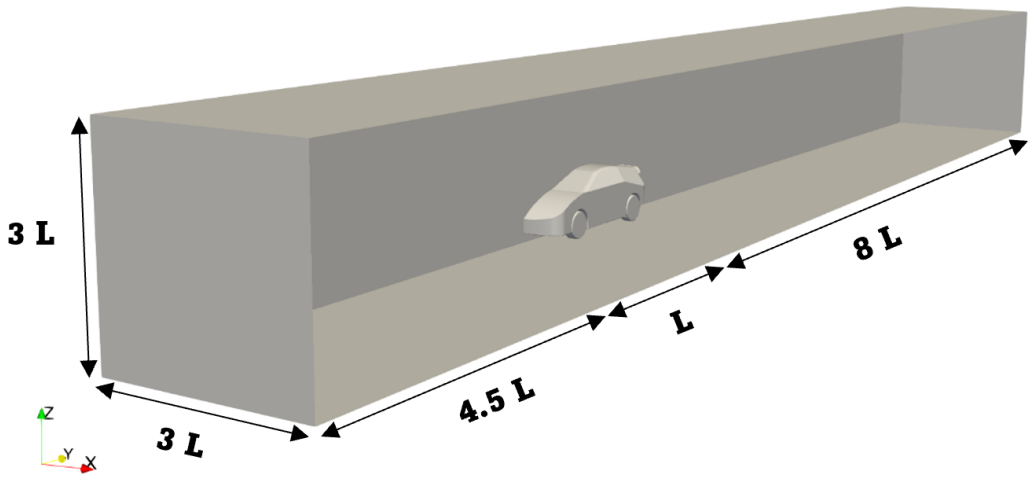

Figure 12. Dimensionless magnitudes of the fluid domain's size.

In regard to the mesh, a three-dimensional unstructured tetrahedral grid was generated using Salome Meca's mesher, as it offers faster mesh generation than the hexahedral approach. Given that the computational resources are limited, this is considered the most suitable option, but the authors are open to future works dealing with a hexahedral grid.

The height of the first cell is set at 0.01 mm with 9 layers at a growth rate of 1.5. The resulting averaged value of y+ was set to 40; therefore, it involved the usage of the so-called wall functions. Additionally, three different refinement regions were defined along with the domain so as to capture the wake development and the viscous effects closer to the vehicle. Special interest was given to the diffuser elements and the edgy floor elements.

Figures 13 and 14 reflect the overall resulting mesh domain. A grid convergence index (GCI) was also used to ensure the independence of the results from the grid size.

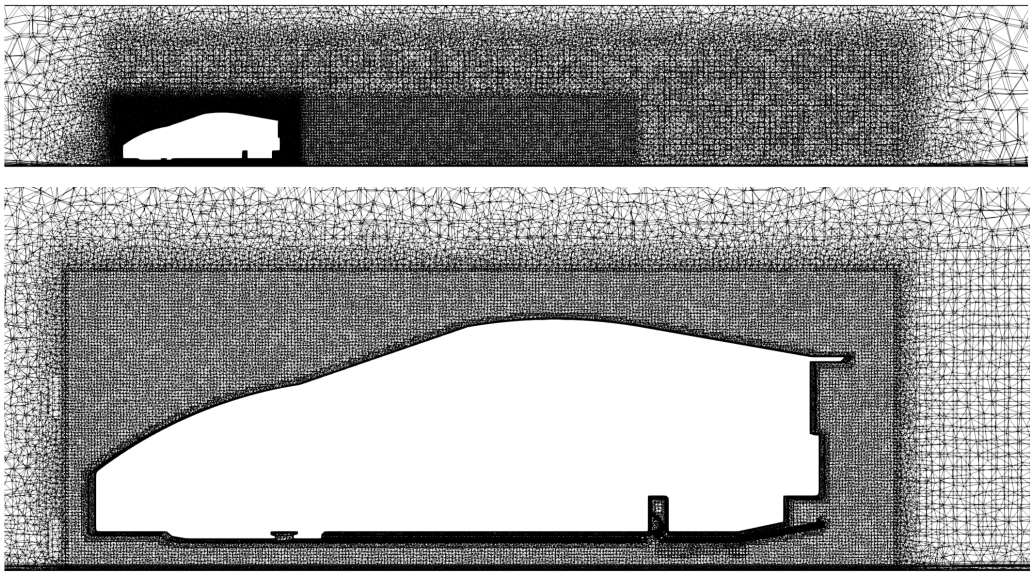

Figure 13. Mesh domain including three local refinement regions.

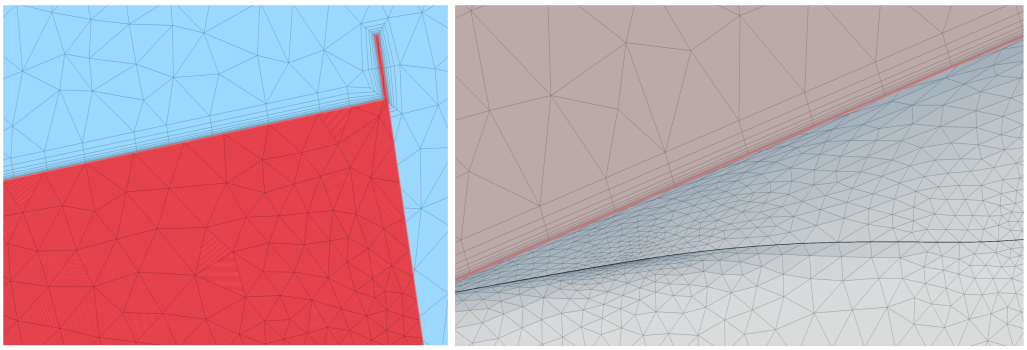

Figure 14. Details of the boundary layers and local refinements.

The GCI methodology was used according to the works of Celik [45]: evaluating three different grid levels at a constant r ratio of elements. The ϕ value selected corresponds to the drag coefficient of the baseline model.

Table 1 presents the main and most relevant results obtained from the GCI analysis.

Table 1. Grid convergence indexes of the three meshes evaluated.

Mesh Parameters	$\phi = C_D$
r_{21}	1.500
r_{32}	1.500
ϕ_1	0.320
ϕ_2	0.310
ϕ_3	0.282
p	2.08
GCI_{fine}	1.218%
GCI_{coarse}	2.928%
A_R	1.032

As can be seen, parameter A_R is definitely close to 1; therefore, it can be stated that the results obtained are in the asymptotic range of convergence [46]. Consequently, the results obtained are independent of the grid size. Computationally, the finest mesh employed contained 6.7 million elements, and the authors considered it reasonable to accept the compromise between the accuracy of the results and the computational resources required to work with such a mesh.

2.4. Boundary and Initial Conditions

The boundary conditions assigned to the problem were:

- Inlet velocity at 25 m/s, a value that can be easily justified in a wind tunnel experiment (for possible future validation purposes).
- Pressure outlet at atmospheric pressure.
- Ground velocity at 25 m/s.
- Symmetry plane (only half of the car was simulated).
- Slip condition on the remaining sidewall and the upper surface.
- Rotating wall at both front and rear wheels (87 rad/s).

As seen in [41], the size of the largest eddy represents the turbulent length scale l, and this can be extrapolated to be the car's wheelbase. Consequently, Table 2 shows the initial conditions of the simulation.

Table 2. Physical variables and initial conditions.

Variable	Value
Free stream velocity U_∞	25 m/s
Fluid density (ρ)	1.225 kg/m^3
Turbulent Intensity (I)	0.150%
Turbulent length scale (l)	0.172 m
Reynolds Number (Re)	$4 \cdot 10^6$

2.5. Simulation Performance

All the simulation operations, including meshing and solver, were performed on a 12-core workstation equipped with 32 Gb of RAM.

Finally, it was considered to have reached convergence when all the residuals of the simulation were below 10^{-5} and the aerodynamic coefficients remained stabilised (around 1000 iterations). Figure 15 shows the convergence plot obtained of the aerodynamic coefficients for the baseline model.

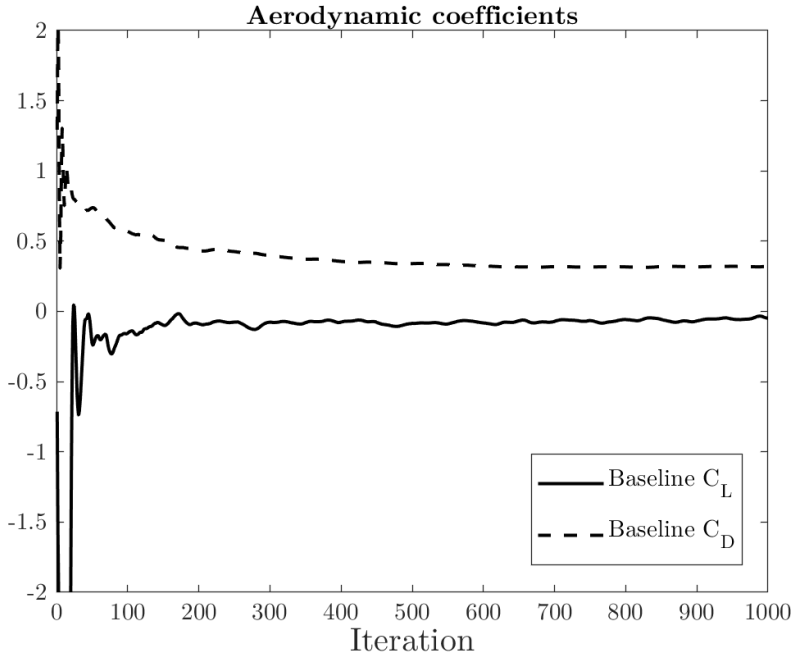

Figure 15. Stability and convergence of the aerodynamic coefficients, baseline model.

The numerical results evaluated deal with both downforce (C_L) and drag (C_D) coefficients and the aerodynamic efficiency (E), defined as the ratio of C_L/C_D.

3. Results and Discussion

Table 3 shows the results of the RANS simulations performed with the four configurations mentioned earlier in the manuscript.

Table 3. Aerodynamic coefficients of the four configurations evaluated.

	Baseline	Venturi Diff.	Venturi Skirts	Venturi Front. Diff.
C_L	−0.047	−0.573	−0.887	−0.773
C_D	0.320	0.325	0.324	0.332
E	−0.146	−1.763	−2.737	−2.323

The C_L of the model had a massive range among the examined configurations: from an insignificant −0.047 for the baseline configuration to a considerable −0.887 for the highest-downforce setup. The baseline model alone barely produced any downforce, a similar result to the one reported in [4], but the addition of the rear diffuser truly made a huge difference. Surprisingly, the addition of the diagonal skirts proved to be more effective than the incorporation of the small frontal diffusers in terms of downforce generation. This could be explained because helping to channelise the airflow towards the big rear diffuser has a higher effect on the creation of aerodynamic loads, as the size of the latter is remarkably greater than that the two geometrical frontal slots. From a manufacturing point of view, it is also a great advantage as the design and implementation of diagonal skirts is significantly easier than sculpting a proper frontal slot close to the tire region.

In regard to the drag coefficient C_D, it can be noted that the addition of the diffuser inherently entails a small increase in the air resistance, from a baseline value of 0.320 up to a 0.332 in the most draggy configuration, just as observed in [4]. However, as observed in the works of Katz et al. [6], the performance achieved with underbody aerodynamics, as opposed to the one obtained with conventional wings, was cleaner regarding wake disturbances and downwash phenomena.

Similarly, the aerodynamic efficiency E experienced an increasing trend when the rear underbody was modified. It can be seen that the most efficient setup is the one involving the venturi skirts, although it involves a higher drag coefficient. A strict evaluation of compromise was performed to consider the trade-off of maximising downforce at the cost of higher flow resistance.

3.1. Velocity Distribution

Figures 16 and 17 reflect the velocity distributions of the four configurations tested. As can be appreciated, the main effect of the diffuser is based on the upwash effect that it produces on configurations (B), (C), and (D), whereas the baseline case (A) shows a less stretched and downwards recirculating zone on the wake. If an overtaking manoeuvre on a circuit was to be performed, configurations (B), (C), and (D) would perform better, as in these configurations, the wake of the car is pushed upwards; therefore, the low-speed flow would remain farther to the nose of the follower car, ensuring less downforce loss as a result of driving closer. This is clearly an advantage when compared to conventional wing downforce generation, which results in a less clean turbulent wake [47].

Among all scenarios, the remarkable effect is that the flow remained attached, which guaranteed that the undertray was working properly with no major stalling issues. Physically, the separation point is where the gradient of the velocity parallel to the wall vanishes perpendicularly to the wall. In Newtonian fluids, flow separation is defined by the sine qua non condition of the wall shear stress value τ_w being equal to zero.

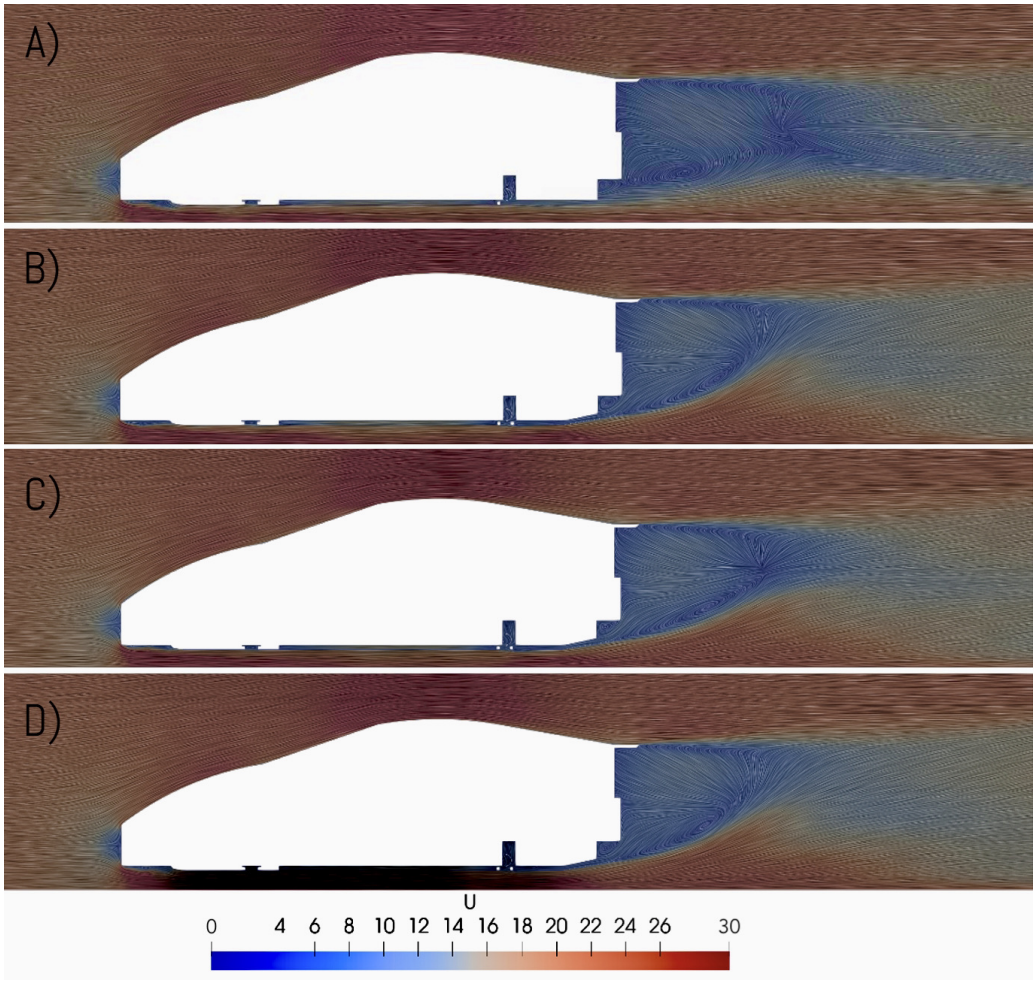

Figure 16. Velocity distribution on the YZ-plane of (**A**) baseline, (**B**) Venturi diffuser, (**C**) Venturi skirt, and (**D**) Venturi frontal configurations. Units are m/s.

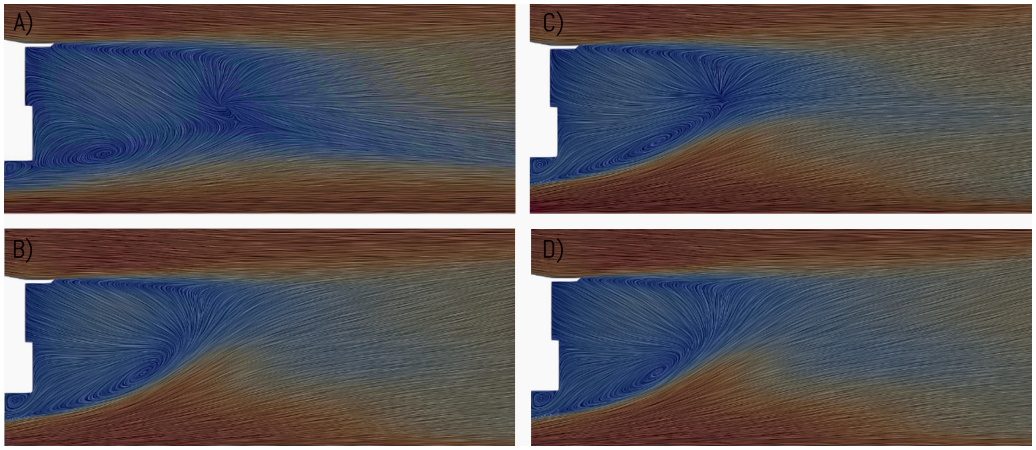

Figure 17. Details of the velocity distributions on the YZ-plane of (**A**) baseline, (**B**) Venturi diffuser, (**C**) Venturi skirts, and (**D**) Venturi frontal configurations.

For visual purposes, Figure 18 shows a three-dimensional iso-contour of the Q criterion coloured by the velocity magnitude around the baseline model. Hunt et al. (1988) [48] described an eddy as the region-zone with a positive second invariant, Q. This is useful to help the reader comprehend not only the shape but also the position and persistency of the three-dimensional vortical structures of such a complex problem.

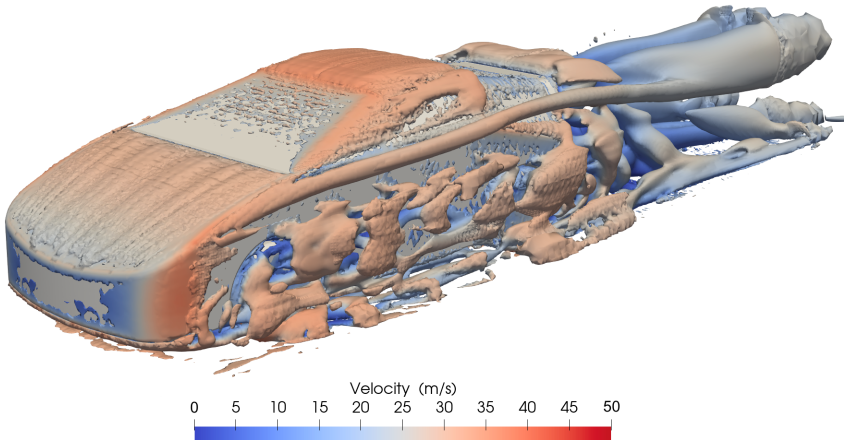

Figure 18. Iso-contour of Q = 50,000 s^{-2} around the baseline configuration.

3.2. Pressure Distribution

Figure 19 shows the pressure contours of the four evaluated configurations. It is rather obvious that the addition of the diffuser in scenarios (B), (C), and (D) generates a much lower pressure area beneath the car that contributes to the generation of the rear downforce.

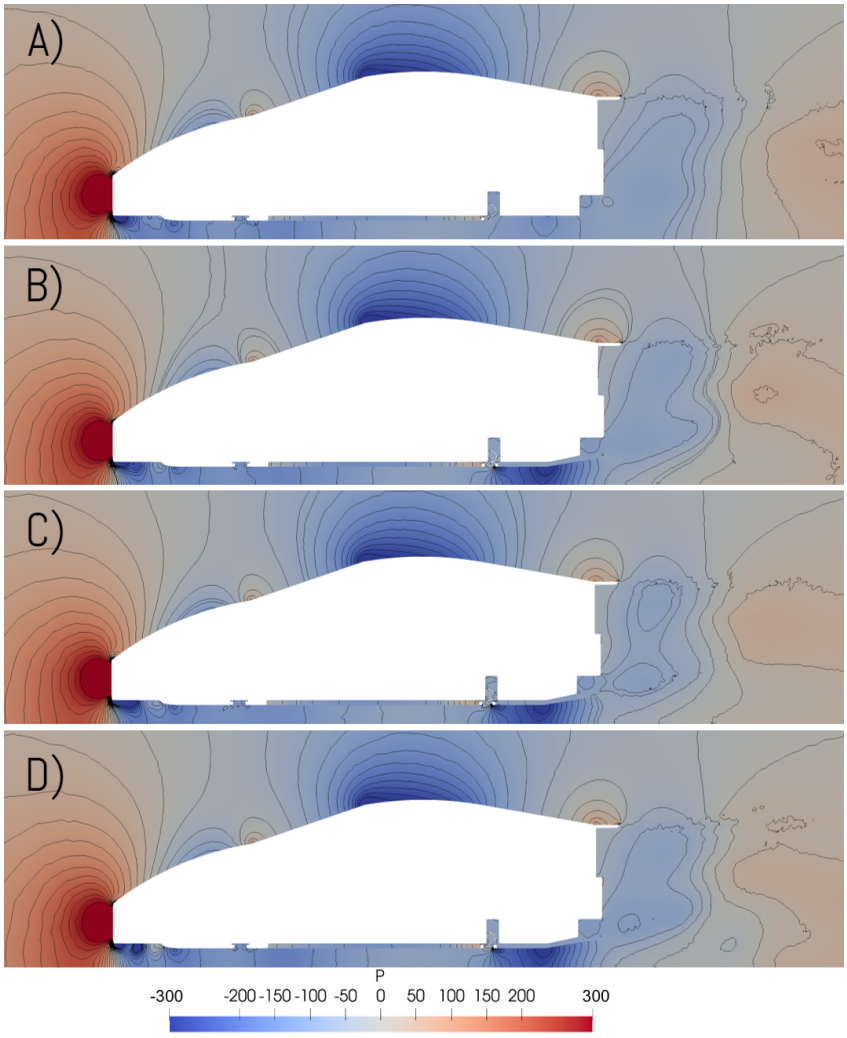

Figure 19. Pressure distribution on the YZ-plane of (**A**) baseline, (**B**) Venturi diffuser, (**C**) Venturi skirts, and (**D**) Venturi frontal configurations. Units are Pa.

Similarly, the pressure distributions on the underbody of the different configurations are shown in Figure 20, where it is possible to appreciate the difference that the diffuser makes. It is interesting, however, to appreciate how configuration (C) channelises the airflow properly by means of the sealing diagonal skirts and enhances the formation of a suction peak in the low-pressure area of the diffuser. The mission of the skirts is two-fold: first, to guide and redirect the flow towards the rear undertray, and second, prevent the outer high-pressure airflow to enter inside the underbody and harm the generation of downforce. Otherwise, the front diffuser slots placed in front of the front tires allow generating and a smooth the low-pressure region that is intended to be treated. In such a way, the airflow runs much smoother around the turbulent rotating areas, creating a non-negligible pressure gradient that must be contemplated when evaluating front balance and the dynamic response of the car.

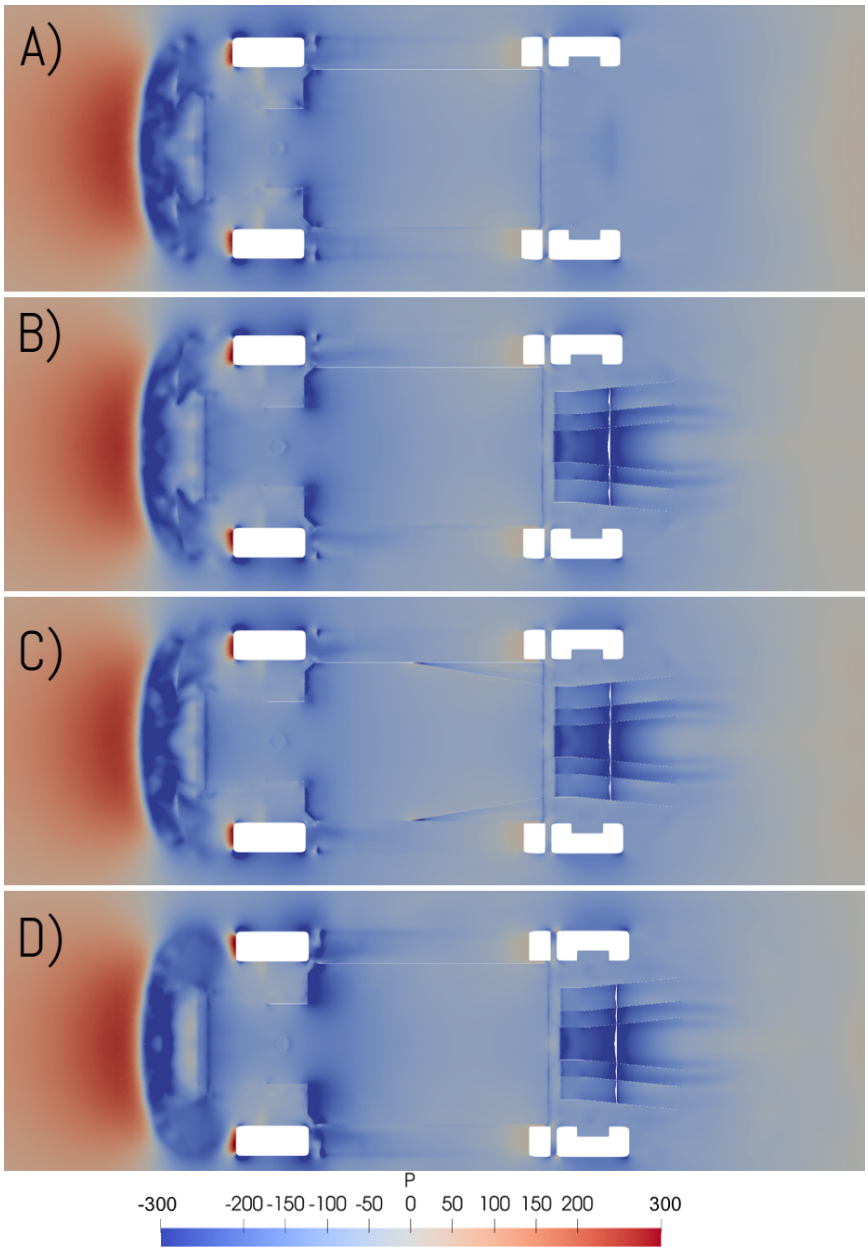

Figure 20. Pressure distribution on the XY-plane of (**A**) baseline, (**B**) Venturi diffuser, (**C**) Venturi skirts, and (**D**) Venturi frontal configurations. Units are Pa.

Figure 21 plots the pressure coefficient values at the rear of the four scenarios studied. The value, which is defined in Equation (1), had the highest peak of pressure in the Venturi skirts configuration, which represents the higher velocity zone [9]. This is in line with it being the highest downforce setup; therefore, the results obtained are reasonable and follow the trend observed in the evaluation of the physical aerodynamic coefficients. In that direction, the other configurations adopted slightly less negative values, the baseline case being the least pronounced of the curves. Finally, it can be seen that the pressure coefficient tends to adopt a value of 0 in all cases at the exit of the underbody, meaning there is a pressure recovery. This pressure recovery is explained as the exit velocity tends to equate the free stream velocity, thereby consolidating that the diffuser configurations are fully functional and operative.

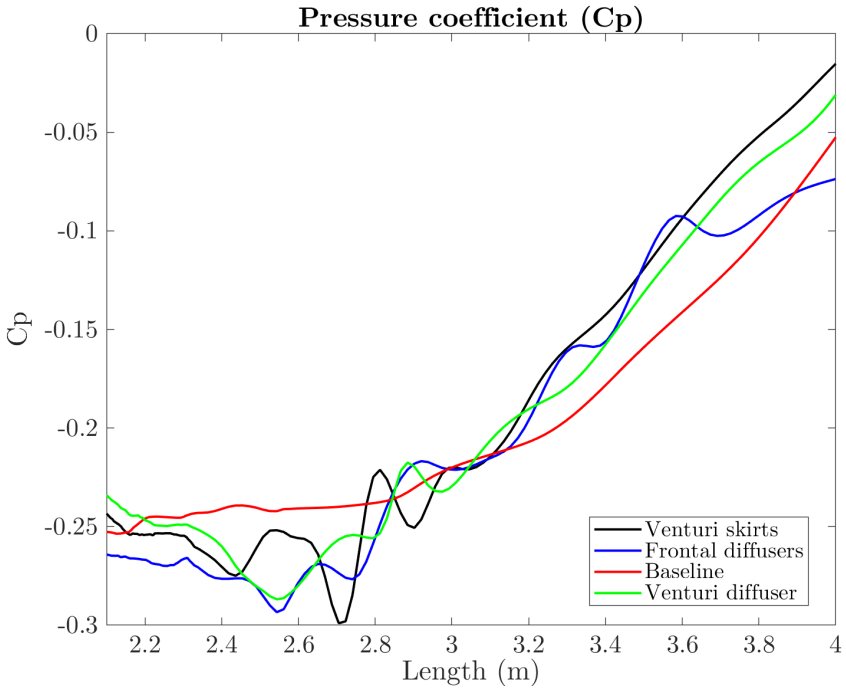

Figure 21. Pressure coefficient distribution along the symmetry plane of the rear undertray.

3.3. Vorticity

Figure 22 presents the vorticity map around the body of the vehicle for the four configurations. As stated in the works of [49], the higher the eddies are at the outer region, the higher the downforce generated. That is perfectly visible in configurations (B), (C), and (D), where the counterclockwise venturi vortices created at the outlet of the diffuser made a huge difference when compared to the baseline configuration (A). It is important to note that configuration (C) can provide a slightly more consistent vorticity gradient on the area close to the body on top of the diffuser. We suggest that it is thanks to the skirts that the airflow remains more attached and consistent through the rear section, as described in [20]. This contrasts with the more abrupt vorticity gradient that can be observed in other configurations, which in turn could result in far less downforce creation.

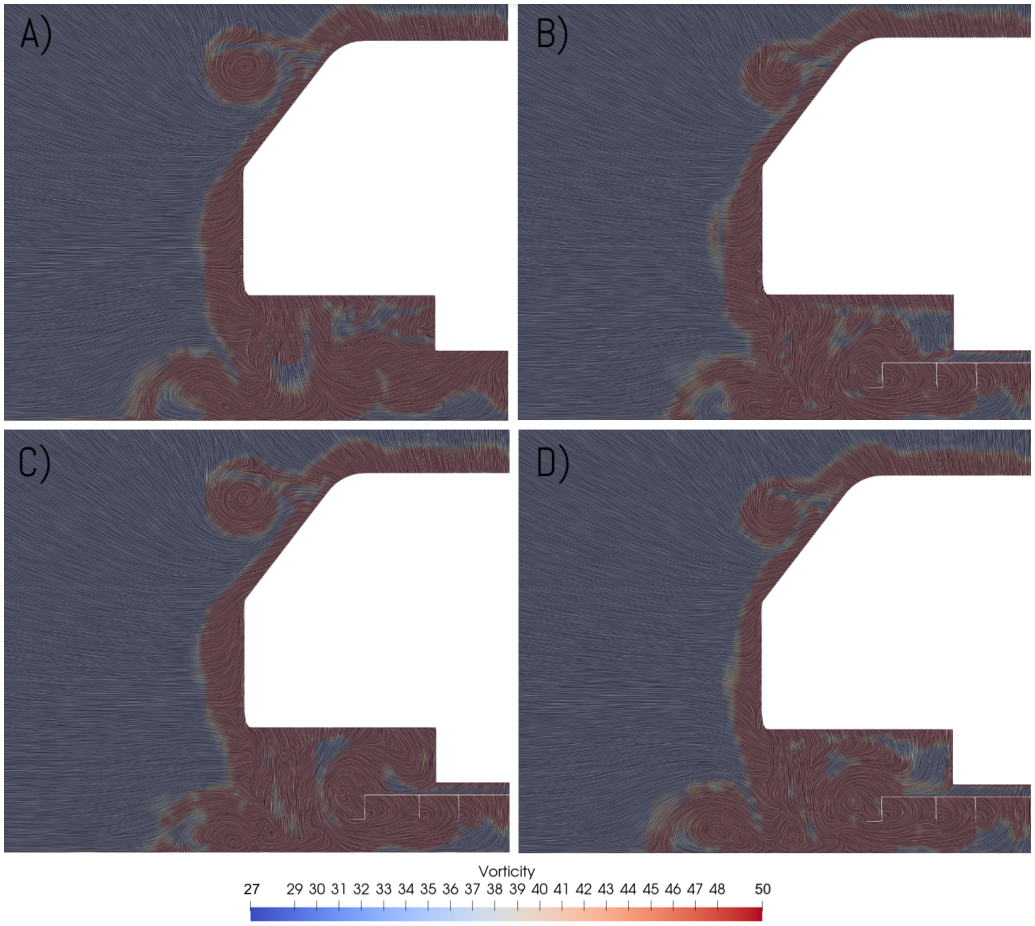

Figure 22. Vorticity map on the XZ-plane of (**A**) baseline, (**B**) Venturi diffuser, (**C**) Venturi skirts, and (**D**) Venturi frontal configurations. Units are s^{-1}.

4. Conclusions

The initial goal of the present manuscript was the study of the effect of rear underbody diffusers on road cars. The understanding of the flow behaviour and the generation of downforce are the two key elements of this work. We presented the novelty of applying slow directly to a realistic road car geometry as opposed to the majority of the available literature, which has used the Ahmed body. Front diffusers research is also rarely reported in the literature; therefore, the results presented here could potentially be valuable for further research.

The design and modification of the rear diffuser of the self-designed baseline model were performed according to the literature review and were based on already published numerical analyses. However, front diffuser design and sealing skirts adaptation were based on the authors' expertise in the field. Consequently, four different configurations were studied, and their aerodynamic coefficients were evaluated. It was observed that the configuration that produced the highest downforce coefficient was the one composed of a 7° venturi diffuser equipped with diagonal sealing skirts, achieving a C_L value of -0.887, which represents an increase of around 1780% with regard to the baseline model. This same configuration also had the highest aerodynamic efficiency E. The other two diffuser configurations (venturi diffuser and venturi frontal diffusers) were stuck between the highest and the lowest downforce scenarios.

Additionally, the two and three-dimensional contours allow for a great understanding of the flow behaviour around the different regions of the car. Studying the wake effects, pressure distribution, and vorticity map could represent a separate line of research, as all this is an extremely complex matter.

The wake behaviour of the diffuser configurations in the velocity field has a smoother and cleaner appearance when compared to the baseline model. The pressure distribution and the pressure coefficient (Cp) displayed a non-subtle change when both front and rear diffusers were employed, including a pronounced spike in low pressure at the starting point of the sealing skirts.

It is important to note that the addition of the diffuser and other aerodynamic devices also contribute to a slightly higher drag coefficient. This finding was clearly observed in the vorticity map and when studying the sizes of the eddies. This must be kept in consideration, although the underbody aerodynamics are cleaner in terms of wake generation.

Future work could involve experimental validation of the presented numerical results or extending the current geometric analysis with new, untested aerodynamic concepts. Unsteady simulations of the same problem would also be useful to test the performances of the solutions we achieved. The authors are aware that some sources of error derived from the numerical RANS approach must have been inherently introduced.

Author Contributions: A.G. and G.E. defined and conceptualized the CAD geometry. A.G. configured and performed the numerical simulations and the analysis of the results. G.E. contributed to the literature review and writing of the manuscript. R.C. reviewed the paper and supervised the work. All authors have read and agreed to the published version of the manuscript.

Funding: This research received no external funding.

Institutional Review Board Statement: Not applicable.

Informed Consent Statement: Not applicable.

Data Availability Statement: Not applicable.

Conflicts of Interest: The authors declare no conflict of interest.

Abbreviations

The following abbreviations are used in this manuscript:

CFD	Computational Fluid Dynamics
FVM	Finite Volume Method
GAMG	Geometric Algebraic Multi Grid
GCI	Grid Convergence Index
CAD	Computer-Aided Design
RAM	Random Access Memory
L	Vehicle length [m]
ϕ	Reference parameter [m^2]
l	Turbulent length scale [m]
I	Turbulent intensity [%]
Re	Reynolds Number
Cp	Pressure coefficient
ρ	Fluid density [kg/m^3]
U_∞	Fluid velocity [m/s]
μ	Dynamic viscosity [kg/m·s]
S	Reference Surface [m^2]
C_L	Lift coefficient
C_D	Drag coefficient
E	Aerodynamic Efficiency

References

1. Katz, J. Aerodynamics of race cars. *Annu. Rev. Fluid Mech.* **2006**, *38*, 27–63. [CrossRef]
2. Hucho, W.; Sovran, G. Aerodynamics of road vehicles. *Annu. Rev. Fluid Mech.* **1993**, *25*, 485–537. [CrossRef]
3. Howell, J.; Sherwin, C.; Passmore, M.; Le Good, G. Aerodynamic drag of a compact SUV as measured on-road and in the wind tunnel. *SAE Trans.* **2002**, *111*, 583–590.
4. Alkan, B. Aerodynamic Analysis of Rear Diffusers for a Passenger Car Using CFD. *engrXiv* **2013**. [CrossRef]

5. Cooper, K.R.; Bertenyi, T.; Dutil, G.; Syms, J.; Sovran, G. The aerodynamic performance of automotive underbody diffusers. *SAE Trans.* **1998**, *107*, 150–179.
6. Katz, J. *Race Car Aerodynamics: Designing for Speed*; R. Bentley: Cambridge, MA, USA, 1995.
7. Ehirim, O.; Knowles, K.; Saddington, A. A review of ground-effect diffuser aerodynamics. *J. Fluids Eng.* **2019**, *141*, 020801. [CrossRef]
8. Porcar, L.; Toet, W.; Gamez-Montero, P.J. Study of the Effect of Vertical Airfoil Endplates on Diffusers in Vehicle Aerodynamics. *Designs* **2021**, *5*, 45. [CrossRef]
9. Huminic, A.; Huminic, G. Computational Study Of Curved Underbody Diffusers. E3S Web of Conferences. *EDP Sci.* **2019**, *128*, 10002.
10. Ahmed, S.R.; Ramm, G.; Faltin, G. Some salient features of the time-averaged ground vehicle wake. *SAE Trans.* **1984**, *93*, 473–503.
11. Hucho, W.H. *Aerodynamics of Road Vehicles: From Fluid Mechanics to Vehicle Engineering*; Elsevier: Amsterdam, The Netherlands, 1987.
12. Gilliéron, P.; Kourta, A. Aerodynamic drag reduction by vertical splitter plates. *Exp. Fluids* **2010**, *48*, 1–16. [CrossRef]
13. Beaudoin, J.F.; Aider, J.L. Drag and lift reduction of a 3D bluff body using flaps. *Exp. Fluids* **2008**, *44*, 491–501. [CrossRef]
14. Ha, J.; Jeong, S.; Obayashi, S. Drag reduction of a pickup truck by a rear downward flap. *Int. J. Automot. Technol.* **2011**, *12*, 369–374. [CrossRef]
15. Zhang, X.; Toet, W.; Zerihan, J. Ground effect aerodynamics of race cars. *Appl. Mech. Rev.* **2006**, *59*, 33–49. [CrossRef]
16. Senior, A.E.; Zhang, X. The force and pressure of a diffuser-equipped bluff body in ground effect. *J. Fluids Eng.* **2001**, *123*, 105–111. [CrossRef]
17. Song, K.S.; Kang, S.O.; Jun, S.O.; Park, H.I.; Kee, J.D.; Kim, K.H.; Lee, D.H. Aerodynamic design optimization of rear body shapes of a sedan for drag reduction. *Int. J. Automot. Technol.* **2012**, *13*, 905–914. [CrossRef]
18. Filipe, F.; Assi, G.R.; Sherwin, S.J.; Meneghini, J.R.; Doorly, D.J. An investigation on the effect of rear underbody diffusers over the flow around automotive bluff bodies. *Imp. Coll. Lond.* **2019**, *2*, 15.
19. Haris, M.N.; Sapit, A.; Mohamed, N.H.N. Study of Airflow Due to Rear Diffuser of Supercar. *J. Complex Flow* **2020**, *2*, 32–36.
20. Cooper, K.R.; Syms, J.; Sovran, G. Selecting automotive diffusers to maximise underbody downforce. *SAE Trans.* **2000**, 497–512. [CrossRef]
21. Ahmed, M.R.; Sharma, S. An investigation on the aerodynamics of a symmetrical airfoil in ground effect. *Exp. Therm. Fluid Sci.* **2005**, *29*, 633–647. [CrossRef]
22. Unni, T.A. *Numerical Investigation on Aerodynamic Effects of Vanes and Flaps on Automotive Underbody Diffusers*; Technical Report, SAE Technical Paper; SAE: Warrendale, PA, USA, 2017.
23. Arun Saha, D.D. *Fluid Mechanics and Fluid Power Contemporary Research*; Springer: Mumbai, India, 2017.
24. Stefano Discetti, A.I. *Experimental Aerodynamics*; CRC Press: Boca Raton, FL, USA, 2017.
25. Toet, W. *William Toet Explains Air Ducts*; Kimberley Media Group: London, UK, 2017.
26. Chandavari, V.; Palekar, S. Diffuser angle control to avoid flow separation. *Int. J. Tech. Res. Appl.* **2014**, *2*, 16–21.
27. Tian, J.; Liu, X.; Zhang, Y.; Chen, Q. *Numerical Analysis of Underbody Diffusers with Different Angles and Channels*; Technical Report, SAE Technical Paper; SAE: Warrendale, PA, USA, 2019.
28. Huminic, A.; Huminic, G. Aerodynamics of curved underbody diffusers using CFD. *J. Wind Eng. Ind. Aerodyn.* **2020**, *205*, 104300. [CrossRef]
29. De Luca, L.T.; Shimada, T.; Sinditskii, V.P.; Calabro, M. *Chemical Rocket Propulsion: A Comprehensive Survey of Energetic Materials*; Springer: Berlin/Heidelberg, Germany, 2016.
30. Howell, J. The influence of a vehicle underbody on aerodynamics of a simple car shapes with an underfloor diffuser. In Proceedings of the Vehicle Aerodynamics, R. Ae. S. Conference, Loughborough, UK, 18–19 July 1994; pp. 36–41.
31. Joseph, P.; Amandolese, X.; Aider, J.L. Drag reduction on the 25 slant angle Ahmed reference body using pulsed jets. *Exp. Fluids* **2012**, *52*, 1169–1185. [CrossRef]
32. Kang, S.O.; Jun, S.O.; Park, H.i.; Song, K.S.; Kee, J.D.; Kim, K.H.; Lee, D.H. Actively translating a rear diffuser device for the aerodynamic drag reduction of a passenger car. *Int. J. Automot. Technol.* **2012**, *13*, 583–592. [CrossRef]
33. Authority, M. Porsche patents active rear diffuser. *Mot. Auth.* **2017**, *12*, 042017.
34. Rasmussen, C.B. Race Car Aerodynamic Design and Optimization via CFD and the Discrete Adjoint Method. Master's Thesis, Aalborg Univeristy Esbjerg, Esbjerg, Denmark, 2018.
35. Huminic, A.; Huminic, G.; Soica, A. Study of aerodynamics for a simplified car model with the underbody shaped as a Venturi nozzle. *Int. J. Veh. Des.* **2012**, *58*, 15–32. [CrossRef]
36. Huminic, A.; Huminic, G. Aerodynamic study of a generic car model with wheels and underbody diffuser. *Int. J. Automot. Technol.* **2017**, *18*, 397–404. [CrossRef]
37. Ruhrmann, A.; Zhang, X. Influence of diffuser angle on a bluff body in ground effect. *J. Fluids Eng.* **2003**, *125*, 332–338. [CrossRef]
38. Asif Ahmed, A.M. CFD analysis of diffuser in a car for downforce generation. *Int. J. Res. Eng. Technol.* **2016**, *5*, 158–164.
39. Senthilkumar, P.; Parthasarathy, M.; Aravind, L.; Narayanan, R.S.; Vegesh, B.; Nelson, D.S. Design and analysis of a rear diffuser in a sedan car. *Mater. Today Proc.* 2021, *in press*. [CrossRef]
40. Constantin, P.; Foias, C. *Navier–Stokes Equations*; University of Chicago Press: Chicago, IL, USA, 1988.
41. Guerrero, A.; Castilla, R. Aerodynamic Study of the Wake Effects on a Formula 1 Car. *Energies* **2020**, *13*, 5183. [CrossRef]
42. Eymard, R.; Gallouët, T.; Herbin, R. Finite volume methods. *Handb. Numer. Anal.* **2000**, *7*, 713–1018.

43. Menter, F.R.; Kuntz, M.; Langtry, R. Ten years of industrial experience with the SST turbulence model. *Turbul. Heat Mass Transf.* **2003**, *4*, 625–632.
44. Broniszewski, J.; Piechna, J. A fully coupled analysis of unsteady aerodynamics impact on vehicle dynamics during braking. *Eng. Appl. Comput. Fluid Mech.* **2019**, *13*, 623–641. [CrossRef]
45. Celik, I. Procedure for Estimation and Reporting of Uncertainty Due to Discretization in CFD Applications. *J. Fluids Eng.* **2008**, *130*, 078001. [CrossRef]
46. NASA. Examining Spatial Grid Convergence. *NASA Gov.* **2021**, *1*, 3.
47. Martins, D.; Correia, J.; Silva, A. The Influence of Front Wing Pressure Distribution on Wheel Wake Aerodynamics of a F1 Car. *Energies* **2021**, *14*, 4421. [CrossRef]
48. Hunt, J. Eddy dynamics and kinematics of convective turbulence. In *Buoyant Convection in Geophysical Flows*; Springer: Berlin/Heidelberg, Germany, 1998; pp. 41–82.
49. Jermann, C.; Pujals, G.; Meliga, P.; Serre, E.; Gallaire, F. Characterization of the streamwise vortices and near-wake dynamics in the turbulent flow around the 25° Ahmed body based on SPIV. In Proceedings of the 3rd GDR Symposium «Flow Separation Control», Ecole Centrale de Lille, Marbella, Spain, 7–8 September 2013.